Materials Research. 2019; 22(3): e20180645
DOI: http://dx.doi.org/10.1590/1980-5373-MR-2018-0645

Influence of CaO Addition, FeO/SiO_2 , and MgO/SiO_2 on the Melting Characteristic Temperatures of FeO-SiO_2 -MgO-CaO System

Yongbo Ma*[a,b], *Xueyan Du*[a,b]

[a]*School of Materials Science and Engineering, Lanzhou University of Technology, 730050, Lanzhou, China*
[b]*State Key Laboratory of Advanced Processing and Recycling of Non-Ferrous Metals, Lanzhou University of Technology, 730050, Lanzhou, China*

Received: October 01, 2018; Revised: December 27, 2018; Accepted: March 09, 2019

In order to decrease the oxidation temperature of fayalite in molten nickel slags, the influence of CaO addition, FeO/SiO_2, and MgO/SiO_2 on melting characteristic temperatures of FeO-SiO_2-MgO-CaO system were investigated. The melting characteristic temperatures, including softening temperature (T_s), hemispherical temperature (T_h), and flow temperature (T_f), were measured with hot stage microscope. Experimental results showed that the melting characteristic temperatures first decreased sharply and then increased slowly with increasing *w*(CaO) for samples at given FeO/SiO_2 and MgO/SiO_2 ratios. The melting characteristic temperatures of samples without CaO addition were much higher than that of samples with different CaO addition, which was mainly caused by the phase components at different compositions. The variation of melting characteristic temperatures were described in detail. Phase components and liquid fractions were calculated by FactSage 7.1, which was good agreement with the XRD patterns.

Keywords: *melting characteristic temperature, nickel slag, FeO/SiO_2, MgO/SiO_2, w(CaO).*

1. Introduction

Nickel slag is the by-product of nickel, for which is widely used in supercapacitor[1] and Ni-based superalloy[2]. A considerable iron-rich nickel slag was thus generated annually. Pyrometallurgical approaches, such as oxidation-magnetic separation[3] and reduction-magnetic method[4], have been proposed for iron recycling from iron-rich nickel slags, and the reaction temperature has always been regarded as a significantly factor. Therefore, more attentions were paid on achieving lower reaction temperature for iron energy-saving recycling.

The investigation of melting characteristic temperatures was performed by both FactSage calculations and optical measurements. FactSage software has been widely used to calculate the phase equilibrium, liquidus temperatures, and solidus temperatures, such as the phase fraction of CaO-Al_2O_3-MgO-SiO_2-CrO_x system[5], the liquidus temperatures of "FeO"-CaO-SiO_2-Al_2O_3-MgO system[6], the liquidus temperatures of SiO_2-MgO-"FeO"-Al_2O_3-CaO system[7], and the phase fractions in copper slag[8]. An optical device was used to measure the characteristic temperatures of CaO-MgO-SiO_2-Al_2O_3 system[9]. The melting properties of SiO_2-CaO-Al_2O_3-B_2O_3-Na_2O samples[10] and the melting behaviors of MgO-SiO_2-Fe_2O_3 slags[11] and CaO-FeO-SiO_2 system[12,13] was performed by a hot-stage microscopy. RDS-05 automatic melting point device was utilized to measure the melting point of CaO-SiO_2-FeO-MgO system in N_2 atmosphere[14].

However, the melting properties of nickel slag, a typical FeO-SiO_2-MgO-CaO system, were merely reported. Therefore, both FactSage software and hot stage microscope were used to investigate the influence of CaO addition, FeO/SiO_2 (F/S), and MgO/SiO_2 (M/S) on the melting characteristic temperatures of FeO-SiO_2-MgO-CaO system in the current work.

2. Materials and Methods

2.1 Materials

Analytical reagents of CaO, Fe, Fe_2O_3, SiO_2, and MgO were used for the sample preparation. Calcium oxide (CaO) powder with a purity of 99.9 % was supplied by Damao Chem Co., Ltd. (Tianjin, China). Reduced iron powder with a purity of 98.0 % was offered by Yantai Chem Co., Ltd. (Yantai, China). Ferric sesquioxide (Fe_2O_3) with a total iron purity of 69.8-70.1 %, silicon dioxide (SiO_2) powder with a purity of 99.0 %, and magnesium oxide (MgO) powder with a purity of 98.0 % was supplied by Kaixin Chem Co., Ltd. (Tianjin, China). Alumina crucibles with a purity of 99.99 %, 90 mm in length, 60 mm in width, 20 mm in height, and 1 mm in thickness, were offered by Jidong Chemical ceramics factory (Tangshan, China).

2.2 Equipment and procedures

A. Equipment

All calculations were performed by using FactSage 7.1 (FACT, Montreal, Canada; GTT Technologies, Aachen, Germany). The FeO-SiO_2-MgO-CaO system was synthesized in

*e-mail: duxy@lut.cn.

a muffle furnace (HTL-1700-80, Haoyue Electric Technology Co., Ltd., Shanghai, China) with an alumina tube (80 mm in diameter × 1000 mm in length). The Hot Stage Microscope (HSM, LZ-III, Northeastern University, Shenyang, China) illustrated in Figure 1(a) was employed to measure the melting characteristic temperatures, where the camera with a 50 mm f/1.8 prime lens was used for photographic recording. The samples were crushed via a grinder (GJ400-1, YongSheng Mineral Equipment Manufacturing Co. Ltd., Ganzhou, China).

B. Sample preparation

According to the composition of nickel slag, the sample compositions were designed, as shown in Table 1. CaO, MgO, SiO_2, Fe, and Fe_2O_3 powders were weighted, mixed, put into an alumina boat and placed it into the center of muffle furnace tube. After purging the furnace by argon at a flow rate of 1.0 L/min for 60 min, the furnace run with a heating rate of 5 K/min to 1673 K, held for 120 min, and cooled naturally to room temperature. Finally, the synthesized samples were

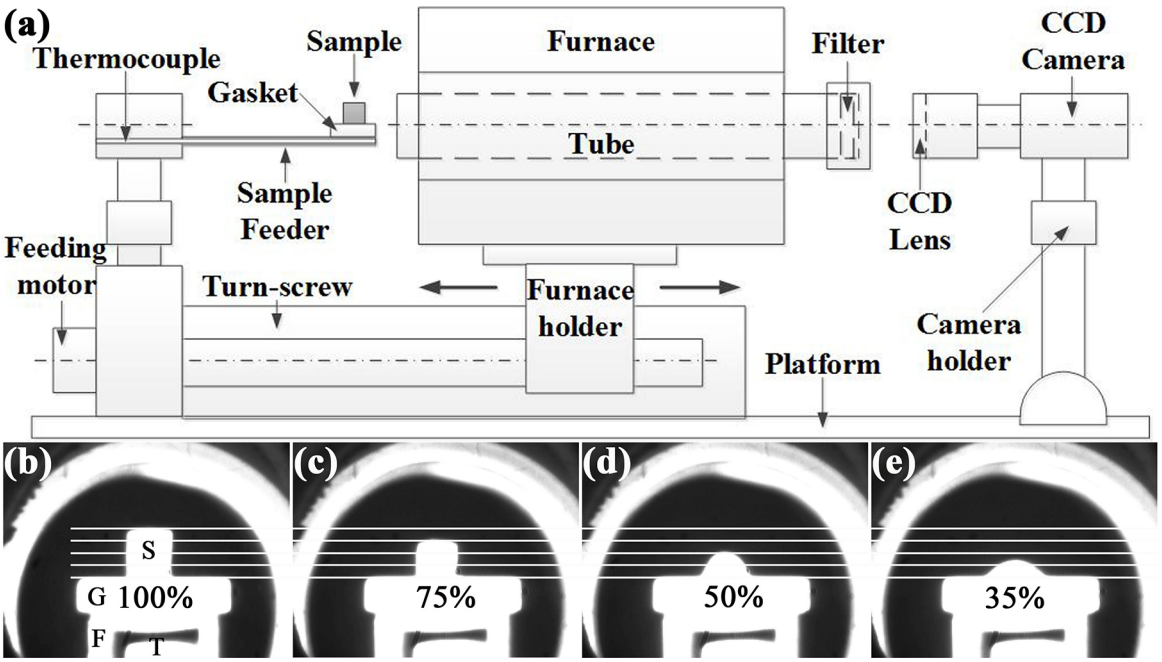

Note: S, G, F, and T in Figure 1(b) denote the sample, gasket, sample feeder, and thermocouple, respectively, shown in Figure 1(a).

Figure 1. Schematic diagram of the Hot Stage Microscope (a) and silhouette photographs (b-e) of samples during the smelting process.

Table 1. Compositions of samples for designed experiments (wt. %).

Sample	F/S	FeO*	SiO_2	MgO	CaO	Sample	F/S	FeO*	SiO_2	MgO	CaO
S1-1	1.33	47.24	35.52	17.24	0.00	**S2-1**	0.40	52.14	34.18	13.67	0.00
S1-2	1.33	44.41	33.39	16.20	6.00	**S2-2**	0.40	49.01	32.13	12.85	6.00
S1-3	1.33	41.57	31.26	15.17	12.00	**S2-3**	0.40	45.88	30.08	12.03	12.00
S1-4	1.33	38.74	29.13	14.13	18.00	**S2-4**	0.40	42.76	28.03	11.21	18.00
S1-5	1.33	35.90	27.00	13.10	24.00	**S2-5**	0.40	39.63	25.98	10.39	24.00
S1-6	1.53	50.66	33.22	16.12	0.00	**S2-6**	0.50	50.66	33.22	16.12	0.00
S1-7	1.53	47.63	31.22	15.15	6.00	**S2-7**	0.50	47.63	31.22	15.15	6.00
S1-8	1.53	44.59	29.23	14.18	12.00	**S2-8**	0.50	44.59	29.23	14.18	12.00
S1-9	1.53	41.55	27.24	13.22	18.00	**S2-9**	0.50	41.55	27.24	13.22	18.00
S1-10	1.53	38.51	25.24	12.25	24.00	**S2-10**	0.50	38.51	25.24	12.25	24.00
S1-11	1.73	53.81	31.10	15.09	0.00	**S2-11**	0.60	48.81	32.00	19.20	0.00
S1-12	1.73	50.58	29.24	14.19	6.00	**S2-12**	0.60	45.88	30.08	18.05	6.00
S1-13	1.73	47.35	27.37	13.28	12.00	**S2-13**	0.60	42.95	28.16	16.89	12.00
S1-14	1.73	44.12	25.50	12.38	18.00	**S2-14**	0.60	40.02	26.24	15.74	18.00
S1-15	1.73	40.89	23.64	11.47	24.00	**S2-15**	0.60	37.09	24.32	14.59	24.00

*Assumed stoichiometric.

crushed into powder in the grinder. The as-synthesized powder of 5.0 g was prepared as columnar samples with a diameter of 3 mm and a height of 3 mm.

C. Measurement of the melting characteristic temperatures

The measurement procedure of melting characteristic temperature was given as follows: first, samples were placed on an alumina gasket and then put it onto the end of sample feeder; subsequently, the furnace at 773 K was moved forward until the given position to ensure samples locating at the center of the furnace; ultimately, height variations of samples were recorded by the camera during the heating process. The first silhouette photograph at 973 K (Figure 1(b)) was defined as the height of 100 %. The T_s, T_h, and T_f were defined as the temperature at which the samples with a height of 75 % (Figure 1(c)), 50 % (Figure 1(d)), and 35 % (Figure 1(e)), respectively.[9,11,13]

3. Results

The measured characteristic temperatures, which were influenced by the composition of samples varied with different F/S ratios and CaO content, were presented in both Table 2 and Figure 2. At given F/S ratios (Figure 2(a), Figure 2(b), and Figure 2(c)), the melting characteristic temperatures all decreased firstly and then increased with increasing of *w*(CaO). When F/S ratio was 1.33 (Figure 2(a)), T_s decreased significantly from 1574 K without CaO addition to 1455 K at 6 wt.% CaO and then slightly decreased to 1452 K at 12 wt.% CaO, and increased to 1466 K at 18 wt.% CaO and 1475 K at 24 wt.% CaO. Similar variation of T_s could also be found for samples with F/S=1.53 (Figure 2(b)), and the lowest value of T_s was 1463 K at 12 wt.% CaO. When F/S was up to 1.73 (Figure 2(c)), T_s decreased from 1496 K without CaO addition to 1450 K at 6 wt.% CaO, and then increased to 1453 K, 1469 K, and 1485 K at 12 wt.% CaO, 18 wt.% CaO, and 24 wt.% CaO, respectively.

T_h for samples with F/S=1.33 (Figure 2(a)) decreased rapidly from 1626 K without CaO addition to 1486 K at 6 wt.% CaO and decreased slowly to1457 K at 12 wt.% CaO. Then, it increased to 1473 K at 18 wt.% CaO and continuously increased to 1488 K at 24 wt.% CaO. Similar variation of T_h could also be observed for samples with F/S=1.53 (Figure 2(b)), and the lowest T_h was 1475 K at 12 wt.% CaO. In addition, when F/S ratio was 1.73 (Figure 2(c)), T_h decreased rapidly from 1634 K at without CaO addition to 1465 K at 12 wt.% CaO, and then increased with further CaO addition.

When F/S ratio was 1.33 (Figure 2(a)), T_f decreased linear from 1641 K at without CaO addition to 1462 K at 12 wt.% CaO and increased linear to 1491 K at 24 wt.% CaO. When F/S ratio was 1.53 (Figure 2(b)), T_f decreased rapidly from 1656 K without CaO addition to 1489 K at 12 wt.% CaO and then decreased slightly to 1486 K at 18 wt.% CaO and continuously up to 1495 K at 24 wt.% CaO. Similar variation of T_f can also be observed when F/S ratio was up to 1.73 (Figure 2(c)).

For specified *w*(CaO) (Figure 2(d), Figure 2(e), and Figure 2(f)), melting characteristic temperatures also varied with increasing F/S ratios. As shown in Figure 2(d), T_s decreased with increasing F/S ratios for samples without CaO addition. However, it decreased obviously with the addition of CaO. With increasing F/S ratios, it increased firstly and then decreased if *w*(CaO) was fixed as 6 wt.%, 12 wt.%, and 18 wt.%, respectively. It was worthwhile to note that T_s for sample with F/S=1.73 was increased gradually if *w*(CaO) was over 6 wt.% CaO. Finally, T_s for samples with F/S=1.73 was higher than that of 1.53 and 1.33, meaning that T_s increased with increasing F/S ratios when *w*(CaO) was specified as 24 wt.%.

As presented in Figure 2(e), T_h for samples without CaO addition increased firstly and then decreased with increasing F/S ratios. It was worth to mention that T_h here were all above 1620 K. It increasing with increasing F/S ratios when *w*(CaO) was increased to 6 wt.% CaO. It was also worthwhile to note that T_h for samples with a CaO content of 6 wt.% was impressively decreased when compared with that of samples without CaO addition. If *w*(CaO) was increased to 12 wt.% CaO and 18 wt.% CaO, a variation of increasing first and decreasing later can be observed for T_h . However, if *w*(CaO) was up to 24 wt.%, T_h increased slightly with increasing F/S ratios.

As shown in Figure 2(f), for samples without CaO addition, T_f changed slightly from 1641 K to 1651K with increasing F/S ratios. When *w*(CaO) was increased to 6 wt.%, it increased linear from 1543 K to 1585 K with increasing F/S ratios. When *w*(CaO) was 12 wt.% and 18 wt.%, T_f increased firstly and then decreased with increasing F/S ratios. When *w*(CaO) was up to 24 wt.% CaO, it increased from 1491 K to 1497 K with increasing F/S ratios.

Meanwhile, the influence of *w*(CaO) and M/S ratios were illustrated in Table 2 and Figure 3. For samples with M/S=0.40 (Figure 3(a)), T_s decreased visibly from 1550 K without CaO addition to 1467 K at 6 wt.% CaO and slightly decreased to 1450 K at 12 wt.% CaO, and then increased to 1457 K and 1480 K at 18 wt.% CaO and 24 wt.% CaO, respectively. Analogously, if M/S ratio was increased to 0.50 (Figure 3(b)) and 0.60 (Figure 3(c)), the same variation of T_s could also be found, and the inflexion points were both observed at 12 wt.% CaO with a temperature of 1460 K and 1463 K, respectively.

T_h for samples with M/S=0.40 (Figure 3(a)) decreased while *w*(CaO) increased from 0 to 18 % and then increased with further CaO addition, where the lowest T_h was 1463 K at 18 wt.% CaO. Similar variation can also be found for samples with M/S ratios of 0.50 (Figure 3(b)) and 0.60 (Figure 3(c)), while the lowest T_h were both found at 12 wt.% CaO with a temperature of 1475 K and 1472 K, respectively.

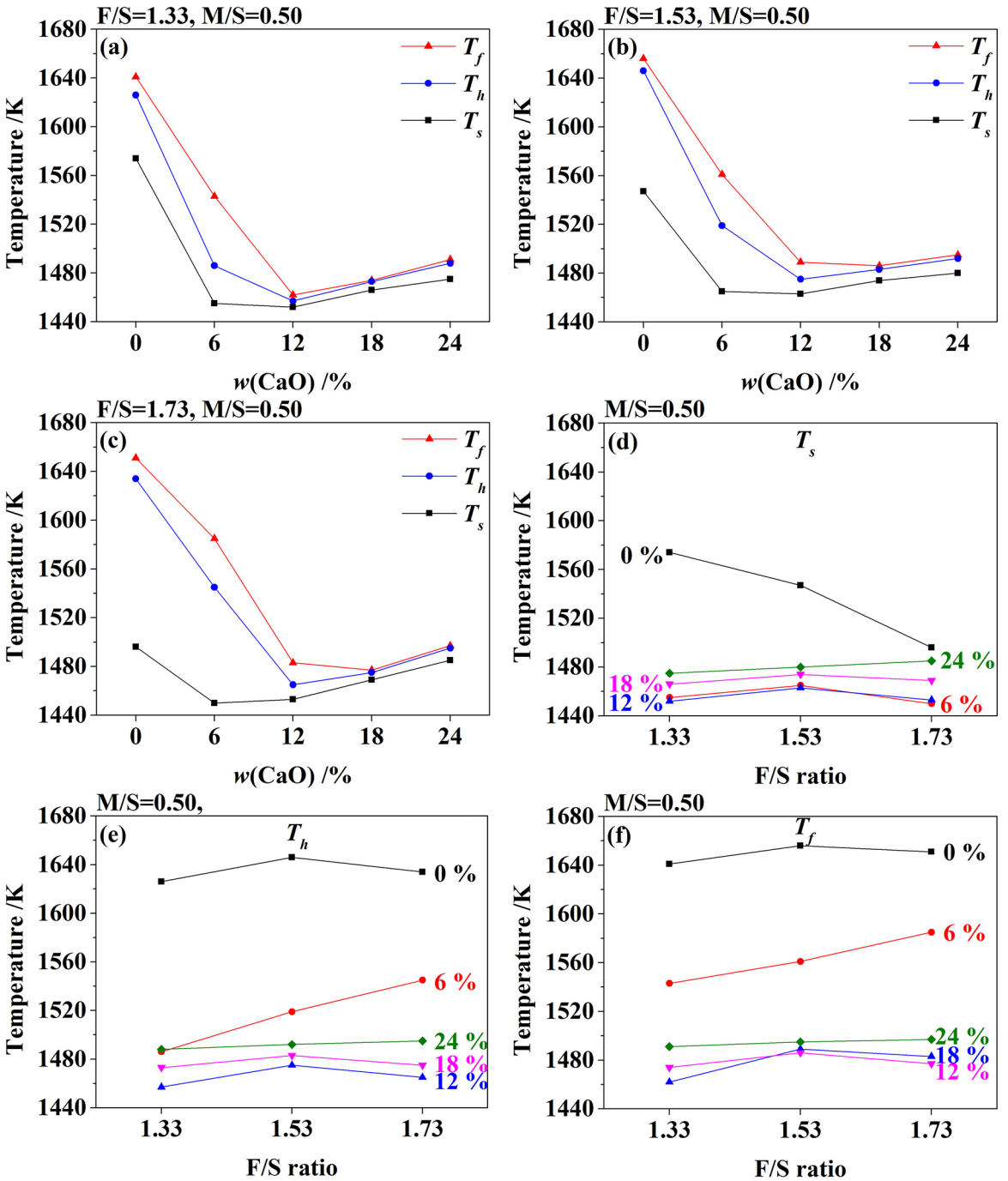

Figure 2. Influence of F/S and *w*(CaO) on the measured characteristic temperatures.

T_f for samples with M/S=0.40 (Figure 3(a)) decreased gradually from 1669 K without CaO addition to 1466 K at 18 wt.% CaO and then increased to 1487 K at 24 wt.% CaO. When M/S ratio was increased to 0.50 (Figure 3(b)), T_f decreased rapidly from 1656 K without CaO addition to 1489 K at 12 wt.% CaO and then slightly decreased to 1486 K at 18 wt.% CaO, it finally increased to 1495 K at 24 wt.% CaO. When M/S ratio was up to 0.60 (Figure 3(c)), the inflexion point of T_f move forward to 12 wt.% CaO with a lowest temperature of 1478 K.

For samples without CaO addition, T_s almost kept a constant, that is 1550 K, with the increasing M/S ratios (Figure 3(d)), and so did T_s (1465 K) at 6 wt.% CaO. When *w*(CaO) was fixed at 12 wt.% and 18 wt.%, T_s increased firstly and then decreased with increasing M/S ratios. Finally, when *w*(CaO)

Table 2. Measured characteristic temperatures for various samples (K).

Sample	T_s	T_h	T_f	Sample	T_s	T_h	T_f
S1-1	1574	1626	1641	**S2-1**	1550	1660	1669
S1-2	1455	1486	1543	**S2-2**	1467	1581	1607
S1-3	1452	1457	1462	**S2-3**	1450	1473	1502
S1-4	1466	1473	1474	**S2-4**	1457	1463	1466
S1-5	1475	1488	1491	**S2-5**	1480	1485	1487
S1-6	1547	1646	1656	**S2-6**	1547	1646	1656
S1-7	1465	1519	1561	**S2-7**	1465	1519	1561
S1-8	1463	1475	1489	**S2-8**	1463	1475	1489
S1-9	1474	1483	1486	**S2-9**	1474	1483	1486
S1-10	1480	1492	1495	**S2-10**	1480	1492	1495
S1-11	1496	1634	1651	**S2-11**	1553	1590	1627
S1-12	1450	1545	1585	**S2-12**	1463	1506	1533
S1-13	1453	1465	1483	**S2-13**	1460	1472	1478
S1-14	1469	1475	1477	**S2-14**	1475	1481	1483
S1-15	1485	1495	1497	**S2-15**	1488	1495	1497

was specified as 24 wt.% CaO, T_s were 1480 K, 1480 K, and 1488 K for samples with M/S ratios of 0.40, 0.50, and 0.60.

For samples without CaO addition (Figure 3(e)), T_h decreased from 1660 K to 1590 K with increasing M/S ratios. When w(CaO) was increased to 6 wt.%, T_h decreased from 1581 K to 1506 K if M/S ratio increased from 0.40 to 0.60. Then, when w(CaO) was specified as 12 wt.%, T_h decreased slightly but almost kept a constant, that was 1473 K, even though M/S increased. It increased from 1463 K to 1483K and then down to 1481 K with increasing M/S ratios when w(CaO) was fixed as 18 wt.%, and finally increased from 1485 K to 1495 K at 24 wt.% CaO.

As illustrated in Figure 3(f), T_f decreased with increasing M/S ratios without CaO addition, 6 wt.% CaO, and 12 wt.% CaO. Then, it increased firstly and then decreased at 18 wt.% CaO with increasing M/S ratios. Finally, it increased with the increasing M/S ratio at 24 wt.% CaO.

4. Discussion

The mentioned above variation of the melting characteristic temperatures may be caused by phase components at different compositions. Therefore, FactSage 7.1 software was used to predict the phase component at different compositions.

4.1 Calculated phase components

Phase components and liquid fractions at equilibrium state for samples with F/S=1.53 and M/S=0.50 were given in Figure 4. When CaO was not added (Figure 4(a)), spinel and orthopyroxene started to crystallize at 1797 K and 1668 K, respectively. When w(CaO) increased to 6 wt.% (Figure 4(b)), spinel, olivine, orthopyroxene, and clinopyroxene crystallized initially at 1803 K, 1659 K, 1591 K, and 1548 K, respectively. It should be mentioned that olivine disappeared at 1559 K. When w(CaO) increased to 12 wt.% (Figure 4(c)), orthopyroxene disappeared and spinel, olivine, and clinopyroxene started to crystallize at 1797 K, 1657 K, and 1575 K, respectively. Clinopyroxene was the sole silicate phase after olivine disappeared at 1568 K. When w(CaO) increased to 18 wt.% (Figure 4(d)), spinel, olivine, melilite, and clinopyroxene crystallized initially at 1779 K, 1615 K, 1606 K, and 1564 K, respectively. The dominant silicate was changed from clinopyroxene to melilite. In addition, when w(CaO) was up to 24 wt.% (Figure 4(e)), clinopyroxene disappeared and phase components were spinel, olivine, and melilite crystallized at 1754 K, 1629 K, and 1640 K, respectively. Melilite was still the dominant phase in the system.

From Figure 4(f), it could be found that the liquid fraction was also influenced by w(CaO). For samples with F/S=1.53 and M/S=0.50, the liquid phase tended to be disappeared at higher temperature with higher w(CaO). For samples without CaO addition, the liquid phase with a SiO_2 content of above 99 wt. % existed stably below 1593 K. But the liquid fraction decreased gradually until 13.34 % at 1453 K for sample with 6 wt.% CaO and it finally disappeared at 1565 K, 1569 K, and 1617 K for samples with a w(CaO) of 12 wt.%, 18 wt.%, and 24 wt.%. This means that the addition of CaO influences both the phase components and liquid fraction.

Moreover, the phase components and liquid phase at equilibrium state for samples with F/S=1.33 and F/S=1.73 when M/S was 0.50 were described in detail in Supplementary

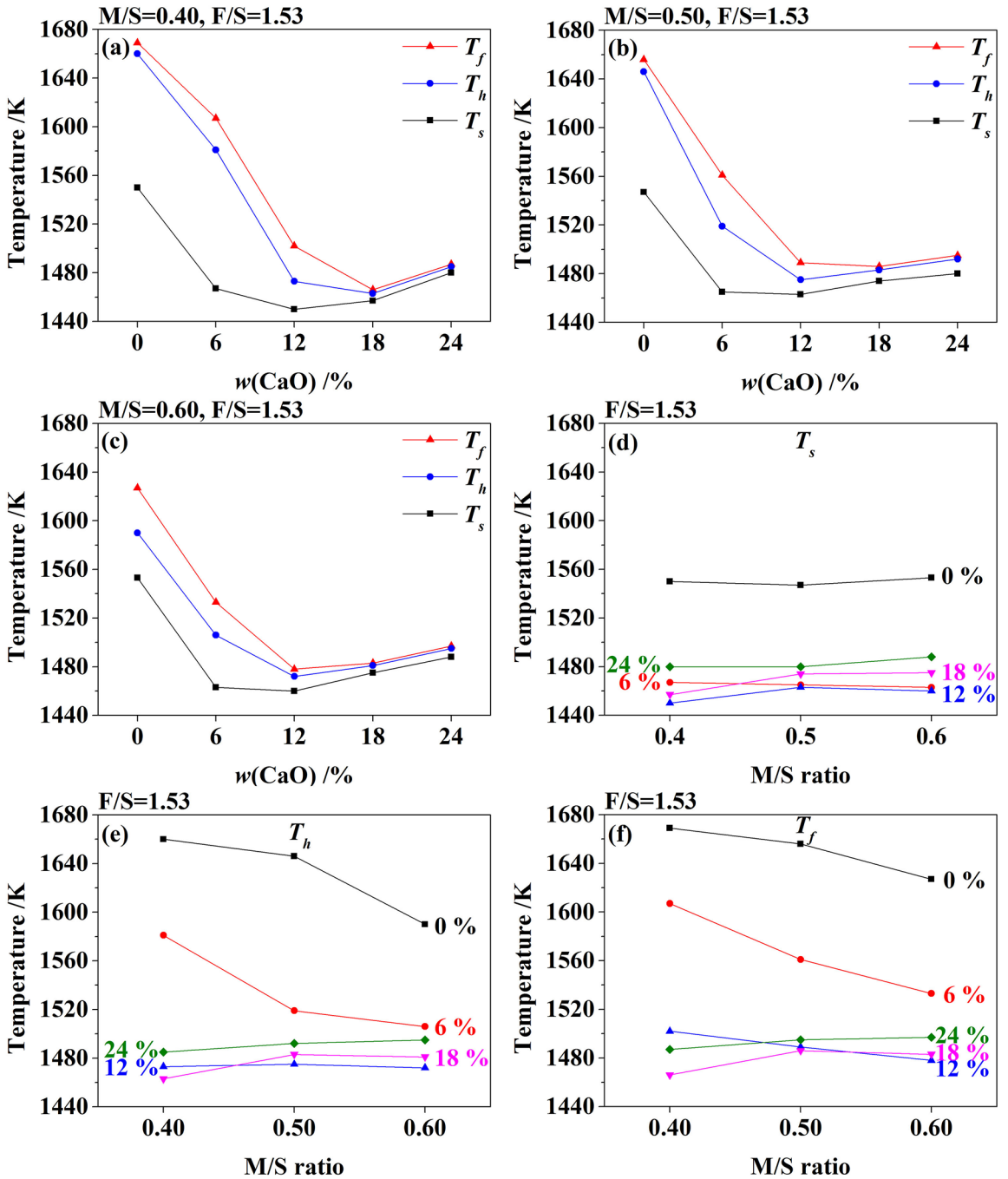

Figure 3. Influence of M/S and *w*(CaO) on the measured characteristic temperatures.

Material (Figure S1 and Figure S2), and that of samples with M/S=0.40 and M/S=0.60 when F/S was 1.53 were also described in detail in Supplementary Material (Figure S3 and Figure S4).

4.3 XRD patterns of typical samples

XRD patterns of samples with F/S=1.53 and M/S=0.50 were shown in Figure 5. It can be found from the XRD patterns that magnetite ($(Fe,Mg)Fe_2O_4$), a type of spinel, is the main iron-bearing phase, while the silicates are significantly affected by the *w*(CaO). When CaO was not added, the system consisted of magnetite and enstatite ($MgSiO_3$), a typical type of orthopyroxene. When *w*(CaO) was 6 wt.%, the silicates were augite ($Ca(Fe,Mg)Si_2O_6$) and forsterite ($(Mg,Fe)_2SiO_4$), corresponding to clinopyroxene and olivine, respectively. Due to the weaker peaks, the predicted orthopyroxene at 6 wt.% CaO and melilite at 12 wt.% CaO were both not observed in the XRD patterns. Monticellite ($CaMgSiO_4$), a member of

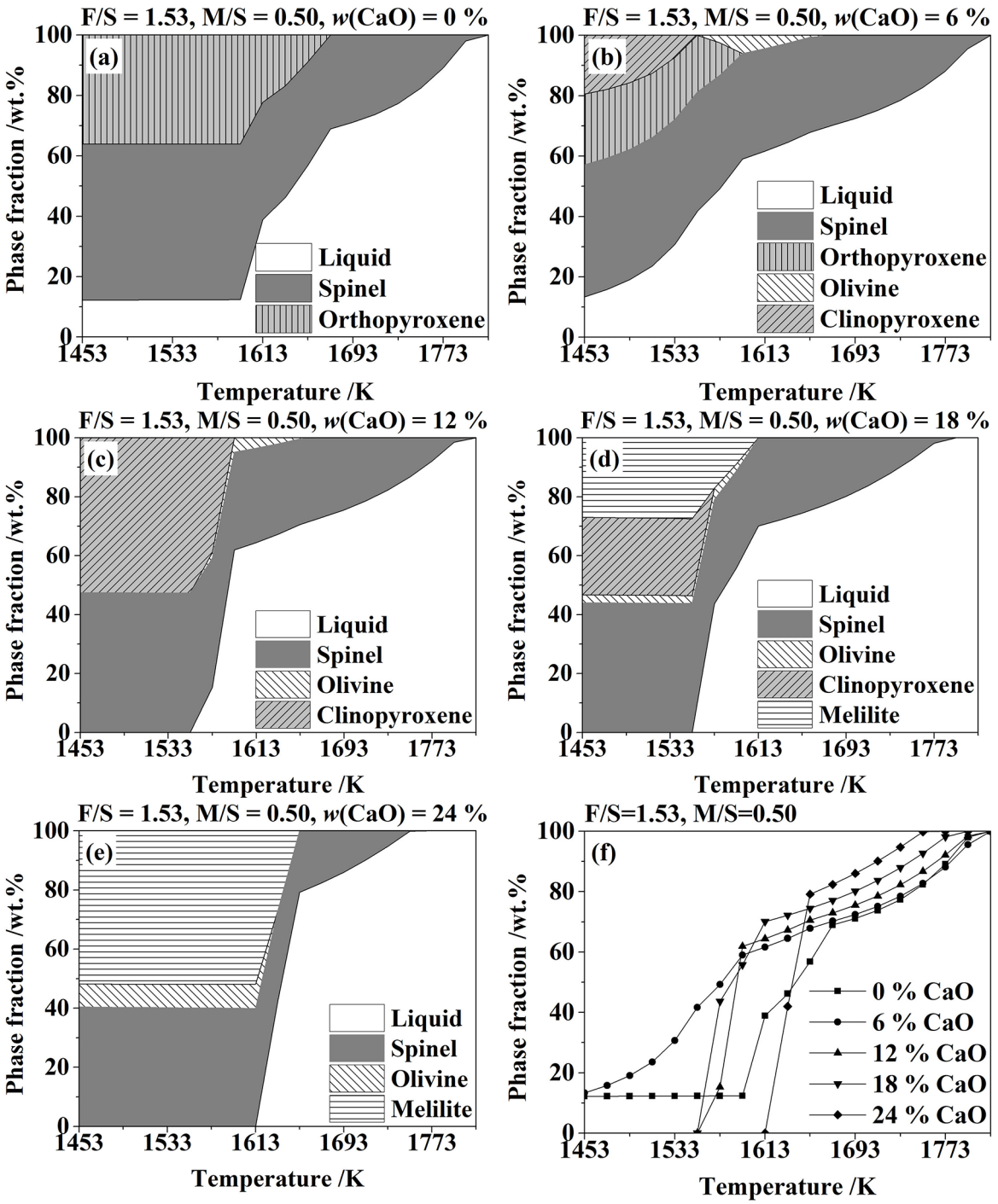

Figure 4. Phase components and liquid fraction at equilibrium state for samples with F/S=1.53 and M/S=0.40.

olivine, formed at 12 wt.% CaO and its peaks strengthened with further CaO addition. When *w*(CaO) was up to 18 %, akermanite ($Ca_2MgSi_2O_7$), a member of melilite, could be obviously discerned. When *w*(CaO) was up to 24 %, weak peaks of augite could be observed in the XRD patterns. In summary, the theoretical calculations are good agreement with the XRD patterns.

5. Conclusions

1. The melting characteristic temperatures all decreased significantly and then increased with increasing *w*(CaO) for samples with given FeO/SiO_2 and MgO/SiO_2 ratios. The melting characteristic temperatures for samples without CaO addition were much higher than those with different CaO addition.

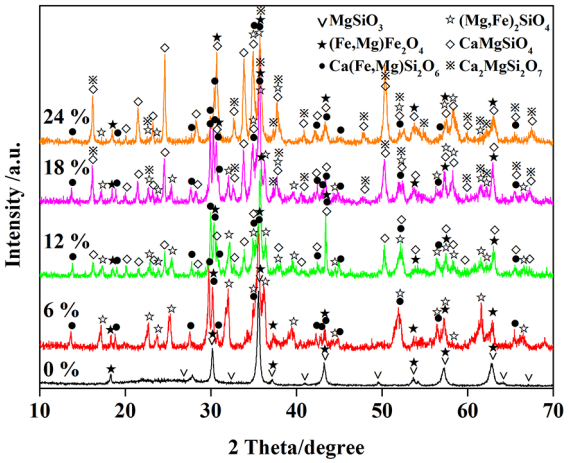

Figure 5. XRD patterns of samples at different *w*(CaO) when F/S and M/S were fixed as 1.53 and 0.50, respectively. **Note**: enstatite ($MgSiO_3$), magnetite ($(Fe,Mg)Fe_2O_4$), augite ($Ca(Fe,Mg)Si_2O_6$), forsterite ($(Mg,Fe)_2SiO_4$), monticellite ($CaMgSiO_4$), and akermanite ($Ca_2MgSi_2O_7$) are the group member of orthopyroxene, spinel, clinopyroxene, olivine, olivine, and melilite, respectively.

2. With increasing F/S, T_s decreased guadually at 0 wt.% CaO, but showed a tendency of increasing firstly but decreasing later at 6 wt.% CaO, 12 wt.% CaO, and 18 wt.% CaO. Moreover, it increased slightly at 24 wt.% CaO. Both T_h and T_f showed a tendency of increasing firstly but decreasing later at 0 wt.% CaO, 12 wt.% CaO, and 18 wt.% CaO, but kept increasing at 6 wt.% CaO and 24 wt.% CaO.
3. With increasing M/S, T_s was almost not influenced for samples without CaO addition and 6 wt.% CaO, but showed a tendency of increasing firstly and decreasing later at 12 wt.% CaO and 18 wt.% CaO. Moreover, it increased gradually at 24 wt.% CaO. Both T_h and T_f decreased at 0 wt.% CaO, 6 wt.% CaO, and 12 wt.% CaO with increasing M/S. T_h increased first and then decreased at 18 wt.% CaO but kept increasing at 24 wt.% CaO with increasing M/S. T_f showed a tendency of increasing firstly but decreasing later at 18 wt.% CaO and increasing at 24 wt.% CaO with increasing M/S.

6. Acknowledgements

The authors are thankful to the Science and Technology Major Project Plan of Gansu Province (145RTSA004) for the financial support.

7. References

1. Wang HY, Liang MM, Duan D, Shi WY, Song YY, Sun ZB. Rose-like Ni3S4 as battery-type electrode for hybrid supercapacitor with excellent charge storage performance. *Chemical Engineering Journal*. 2018;350:523-533.
2. He DG, Lin YC, Jiang XY, Yin LX, Wang LH, Wu Q. Dissolution mechanisms and kinetics of δ phase in an aged Ni-based superalloy in hot deformation process. *Materials & Design*. 2018;156:262-271.
3. Ma YB, Du XY, Shen YY, Li GZ, Li M. Crystallization and Beneficiation of Magnetite for Iron Recycling from Nickel Slags by Oxidation-Magnetic Separation. *Metals*. 2017;7(8):321-332.
4. Ni W, Jia Y, Zheng F, Wang ZJ, Zheng MJ. Comprehensive utilization of iron recovery from Jinchuan nickel residue. *Journal of University of Science and Technology Beijing*. 2010;32(8):975-980.
5. Shu QF, Luo QY, Wang LJ, Chou KC. Effects of MnO and CaO/SiO2 mass ratio on phase formations of $CaO-Al_2O_3-MgO-SiO_2$-CrOx slag at 1673K and $P_{O2}=10^{-10}$ atm. *Steel Research International*. 2015;86(4):391-399.
6. Jang KO, Ma XD, Zhu JM, Xu HF, Wang G, Zhao BJ. Phase Equilibria in the System "FeO"-CaO-SiO_2-Al_2O_3-MgO at Different CaO/SiO_2 Ratios. *Metallurgical and Materials Transaction B*. 2017;48(3):1547-1560.
7. Ma XD, Cui ZX, Zhao BJ. Efficient utilization of nickel laterite to produce master alloy. *JOM*. 2016;68(12):3006-3014.
8. Heo JH, Kim BS, Park JH. Effect of CaO Addition on Iron Recovery from Copper Smelting Slags by Solid Carbon. *Metallurgical and Materials Transaction B*. 2013;44(6):1352-1363.
9. Talapaneni T, Yedla N, Sarkar S, Pal S. Effect of basicity, Al2O3 and MgO content on the softening and melting properties of the CaO-MgO-SiO2-Al_2O_3 high alumina quaternary slag system. *Metallurgical Research & Technology*. 2016;113(5):501-511.
10. Wang L, Zhang C, Cai DX, Zhang JQ, Sasaki Y, Ostrovski O. Effects of CaO/SiO_2 Ratio and Na_2O Content on Melting Properties and Viscosity of SiO_2-CaO-Al_2O_3-B_2O_3-Na_2O Mold Fluxes. *Metallurgical and Materials Transaction B*. 2017;48(1):516-526.
11. Sagadin C, Luidold S, Wagner C, Wenzl C. Melting Behaviour of Ferronickel Slags. *JOM*. 2016;68(12):3022-3028.
12. Ueda S, Kon T, Miki T, Kim SJ, Nogami H. Effects of Al_2O_3 and MgO on Softening, Melting, and Permeation Properties of CaO-FeO-SiO_2 on a Coke Bed. *Metallurgical and Materials Transaction B*. 2016;47(2):2371-2377.
13. Ueda S, Kon T, Miki T, Kim SJ, Nogami H. Softening, Melting, and Permeation Phenomena of CaO-FeO-SiO_2 Oxide on a Coke Bed. *ISIJ International*. 2015;55(10):2098-2104.
14. Zhao JX, Zhao ZY, Cui YR, Shi RM, Tang WD, Li XM, et al. New Slag for Nickel Matte Smelting Process and Subsequent Fe Extraction. *Metallurgical and Materials Transaction B*. 2018;49(1):304-310.

Supplementary material

The following online material is available for this article:

Figure S1Effects of *w*(CaO) on the phase fractions of samples with F/S=1.33 at equilibrium state.

Figure S2Effects of *w*(CaO) on the phase fractions of samples with F/S=1.73 at equilibrium state.

Figure S3Effects of *w*(CaO) on the phase fractions of samples with M/S=0.40 at equilibrium state.

Figure S4Effects of *w*(CaO) on the phase fractions of samples with M/S=0.60 at equilibrium state.